Published in final edited form as:
Biochemistry. 2010 October 19; 49(41): 8839–8846. doi:10.1021/bi101201c.

Contribution of Subdomain Structure to the Thermal Stability of the Cholera Toxin A1 Subunit†

Tuhina Banerjee[‡], **Abhay Pande**[‡,§], **Michael G. Jobling**[‖], **Michael Taylor**[‡], **Shane Massey**[‡,⊥], **Randall K. Holmes**[‖], **Suren A. Tatulian**[‡‡], and **Ken Teter**[‡,*]

[‡]Burnett School of Biomedical Sciences, College of Medicine, University of Central Florida, Orlando, Florida 32826

[‖]Department of Microbiology, University of Colorado Denver School of Medicine, Aurora, CO 80045

[‡‡]Department of Physics, University of Central Florida, Orlando, Florida 32816

Abstract

The catalytic A1 subunit of cholera toxin (CTA1) is an ADP-ribosyltransferase with three distinct subdomains: $CTA1_1$ forms the catalytic core of the toxin; $CTA1_2$ is an extended linker between $CTA1_1$ and $CTA1_3$; and $CTA1_3$ is a compact globular region. CTA1 crosses the endoplasmic reticulum (ER) membrane to enter the cytosol where it initiates a cytopathic effect. Toxin translocation involves ER-associated degradation (ERAD), a quality control system that exports misfolded proteins from the ER to the cytosol. At the physiological temperature of 37°C, the free CTA1 subunit is in a partially unfolded conformation that triggers its ERAD-mediated translocation to the cytosol. Thus, the temperature sensitivity of CTA1 structure is an important determinant of its function. Here, we examined the contribution of CTA1 subdomain structure to the thermal unfolding of CTA1. Biophysical measurements demonstrated that the $CTA1_1$ subdomain is thermally unstable, and that the $CTA1_2$ subdomain provides a degree of conformational stability to $CTA1_1$. The $CTA1_3$ subdomain does not affect the overall stability of CTA1, but the thermal unfolding of CTA1 appears to begin with a local loss of structure in the $CTA1_3$ subdomain: glycerol and acidic pH both inhibited the thermal disordering of full-length CTA1 but not the disordering of a CTA1 construct lacking the $A1_3$ subdomain. These observations provide mechanistic insight regarding the thermal unfolding of CTA1, an event which facilitates its subsequent translocation to the cytosol.

Cholera toxin (CT)1 is an AB protein toxin that contains an enzymatic A moiety and a cell-binding B moiety (1,2). Many plant and bacterial toxins share this general structural

†This work was supported by National Institutes of Health grants R03 AI067987 to K. Teter, R01 AI073783 to K. Teter, and R01 AI031940 to R.K. Holmes.

*To whom correspondence should be addressed: Tel. (407) 882-2247; Fax: (407) 384-2062; kteter@mail.ucf.edu.
§Present address: Department of Biotechnology, National Institute of Pharmaceutical Education and Research (NIPER), Sec-67, S.A.S. Nagar (Mohali)-160062, India
⊥Present address: Department of Microbiology and Immunology, University of Texas Medical Branch, Galveston, Texas 77555

SUPPORTING INFORMATION AVAILABLE

A table of ΔH values, a table of unfolding data for reduced CTA1/CTA2, locations of CTA1 tryptophan and tyrosine residues in ribbon diagrams and space-filling models, assessment of protein purification by SDS-PAGE, the full series of His_6-tagged CTA1 biophysical measurements from 18°C to 55°C, the thermal unfolding of a reduced CTA1/CTA2 heterodimer at pH 6.0 and 7.5, and experiments demonstrating the cellular effects resulting from acid-induced stabilization to the tertiary structure of CTA1 are provided as Supporting Information. This material is available free of charge via the Internet at http://pubs.acs.org.

[1]Abbreviations: CT, cholera toxin; CTA1, the catalytic A1 subunit of CT; CD, circular dichroism; ER, endoplasmic reticulum; ERAD, ER-associated degradation; SDS-PAGE, sodium dodecyl sulfate polyacrylamide gel electrophoresis; T_m, transition temperature; λ_{max}, peak fluorescence wavelength

organization. In the case of CT, the B subunit is a homopentameric ring-like structure that binds to GM1 gangliosides on the eukaryotic plasma membrane. The CTA subunit is initially produced as a single polypeptide of 240 amino acid residues, and it is then proteolytically cleaved at residue 192 to generate a disulfide-linked A1/A2 heterodimer. CTA1 is a 22 kDa ADP-ribosyltransferase with three distinct subdomains: $CTA1_1$ (residues 1 to 132) is the globular, compact catalytic core of the toxin; $CTA1_2$ (residues 133 to 161) wraps around the $A1_1$ subdomain and forms an extended bridge which links $CTA1_1$ with $CTA1_3$; and $CTA1_3$ (residues 162 to 192) is a globular region with many hydrophobic residues and the cysteine residue which covalently tethers CTA1 to CTA2 (3,4). The 5.5 kDa CTA2 subunit consists of an α-helix that abuts the CTA1 subunit and an elongated C-terminal tail that sits within the central cavity of the B pentamer (5). CTA2 maintains numerous non-covalent interactions with CTB, thereby connecting the cell-binding and catalytic components of the toxin.

CT travels as an intact AB holotoxin from the cell surface to the endoplasmic reticulum (ER) (6). The disulfide bond linking CTA1 to CTA2 is reduced in the ER (7,8), which then permits the chaperone-dependent dissociation of CTA1 from $CTA2/CTB_5$ (9). CTA1 is kept in a folded conformation when associated with other components of the CT holotoxin (10–12), but it shifts to a partially unfolded state when released from $CTA2/CTB_5$ at physiological temperature (11). This conformational change identifies the dissociated CTA1 subunit as a misfolded protein for processing by the quality control mechanism of ER-associated degradation (ERAD) (13). ERAD is a normal cellular process that recognizes misfolded or misassembled proteins in the ER and exports them to the cytosol for degradation by the ubiquitin-proteasome system (14). CTA1 evades ubiquitin-dependent proteasomal degradation after its translocation to the cytosol because the toxin has a dearth of lysine residues for ubiquitin conjugation (11,15,16). An interaction with ADP-ribosylation factors and possibly other cytosolic proteins allows the translocated pool of CTA1 to attain an ordered, active conformation which could further help it resist proteasomal degradation (11,17,18). The refolded CTA1 subunit subsequently modifies its Gsα target to elicit a cytopathic effect. Other AB toxins such as ricin and Shiga toxin also exploit ERAD for A chain translocation to the cytosol (19).

The thermal instability of the isolated CTA1 subunit plays an essential role in toxin translocation to the cytosol. However, the relationship between CTA1 subdomain structure and CTA1 thermal instability has not been examined. In addition, the process of CTA1 thermal unfolding remains uncharacterized. To address these issues, we analyzed the structural characteristics of CTA1, a CTA1 construct lacking most of the $A1_3$ subdomain ($CTA1_{1–168}$), and a CTA1 construct lacking both the $A1_2$ and $A1_3$ subdomains ($CTA1_{1–133}$). Our data indicate that the $A1_1$ subdomain alone is thermally unstable, that the $A1_2$ subdomain provides a degree of conformational stability to $CTA1_1$, and that the $CTA1_3$ subdomain does not affect overall toxin stability. Our data also suggest that the thermal unfolding of CTA1 begins with a localized loss of structure in the $A1_3$ subdomain. These results provide insight into the molecular mechanism of CTA1 unfolding, a key event for ERAD-mediated toxin translocation to the cytosol and cellular intoxication.

EXPERIMENTAL PROCEDURES

Structural studies

The temperature-dependent unfolding of CTA1 was studied with a J-810 spectrofluoropolarimeter (Jasco Corp., Tokyo, Japan) and a Jasco PFD-425S Peltier temperature controller. Experiments were performed with a 4-mm optical path-length rectangular quartz cuvette. The protein concentrations of His-tagged CTA1 constructs were 70 μg in 220 μL of 20 mM sodium borate buffer (pH 7.0) containing 100 mM NaCl. Protein

concentration of the commercially available CTA1/CTA2 heterodimer (Calbiochem, La Jolla, CA) was 34 μg in 200 μL of 20 mM sodium phosphate buffer (pH 6.0 or 7.5) containing 150 mM NaCl and, to reduce the heterodimer, 10 mM β-mercaptoethanol. Thermal unfolding was carried out in the temperature range of 18–55°C, and samples were allowed to equilibrate for 4 min at each temperature before measurement. For fluorescence spectra, CTA1 tryptophan residues were excited at 290 nm and the fluorescence emission was measured between 300 and 400 nm. Circular dichroism (CD) spectra were recorded from 190 to 320 nm, which covers both near-UV and far-UV range, and were averaged from 5 scans. The same sample was used for all measurements to eliminate possible errors resulting from sample-to-sample variability. For CD measurements, the observed ellipticity was converted to mean residue molar ellipticity, [θ], in units of degrees×cm^2×dmol^{-1} using

$$[\theta] = \frac{\theta_{obs}}{c n_{res} l} \tag{1}$$

where θ_{obs} is the measured ellipticity in millidegrees, c is the molar concentration of the protein, n_{res} is the number of amino acid residues in the protein, and l is the optical path-length in millimeters.

The thermal profiles of conformational changes in the protein, as determined by CD and fluorescence spectroscopy and plotted in Figures 2–5, were fitted with simulated curves using the following equation (22):

$$X = f_L X_L + (1 - f_L) X_H \tag{2}$$

where X is the ellipticity or the fluorescence measured at a given temperature, f_L is the fraction of amino acids representing the native conformation at low temperature, X_L and X_H are limiting values of X at low and high temperatures, respectively. The parameter, f_L, is given by

$$f_L = \frac{exp(-\Delta G/RT)}{1+exp(-\Delta G/RT)} \tag{3}$$

where the temperature dependence of the free energy of unfolding (ΔG) is described by

$$\Delta G = \Delta H \left(1 - \frac{T}{T_m}\right) + \Delta C \left[T - T_m - T\ ln\left(\frac{T}{T_m}\right)\right] \tag{4}$$

T is the absolute temperature, T_m is the transition temperature (i.e., the midpoint of transition between folded and unfolded states), ΔH is the apparent enthalpy of unfolding, and ΔC is the heat capacity of unfolding. The parameter ΔC = 0.39 kcal mol^{-1}K^{-1} was used, consistent with our earlier data (11). Values of ΔH that were used to obtain the best fit between experimental and simulated curves are listed in Supporting Information Table S1. The locations of CTA1 tryptophan and tyrosine residues, which impact fluorescence and near-UV CD measurements, are shown in Supporting Information Figure S1. Replicate experiments with CTA1 and CTA1$_{1–168}$ indicated that the T_m values did not deviate by more than 1°C.

CTA1 constructs

The construction and purification of His-tagged CTA1 and $CTA1_{1–168}$ were previously described (20,21). A clone expressing His-tagged $CTA1_{1–133}$ was made by PCR amplification from the full-length His-tagged CTA1 template in pT7CTA1h6 (21) with a T7 vector primer and TCAGAATTCCCAAAATGAACTCGATACC primer that appended an EcoRI site encoding Asn-Ser after residue Gly-133. An XbaI-EcoRI digest of this PCR fragment was cloned back into pT7CTA1h6 in place of the full-length CTA1 coding sequence. The predicted DNA sequence was confirmed. $CTA1_{1–133}$ encodes a protein ending with Gly-133 followed by the NSHHHHHH tag and was purified as previously described (20,21). Although the presence of the His_6 tag could affect the absolute T_m value and its pH dependence, each CTA1 construct had the same C-terminal His_6 tag so experimental differences between them should not reflect the presence of the tag. The CTA1 preparations were resolved by sodium dodecyl sulfate polyacrylamide gel electrophoresis (SDS-PAGE) and visualized with Coomassie staining in order to confirm the purity of the protein preparations (Supporting Information Fig. S2).

In order to facilitate protein refolding, the purified toxins were dialyzed against five changes of 500 mL of 20 mM sodium borate buffer (pH 7.0) containing 100 mM NaCl before experimental use. The first step was for 2 h at 4°C in 6 M urea buffer; the second step was for 2 h at 4°C in 2 M urea buffer; the third step was for 2 h at 4°C in 1 M urea buffer; the fourth step was for 2 h at 4°C in urea-free buffer; and the last step was again for 2 h at 4°C in urea-free buffer. Slide-a-lyzer 3500 MWCO dialysis cups (Pierce, Rockford, IL) were used for the procedure. After dialysis, the His-tagged toxins were used immediately.

RESULTS

Organization and stability of the CTA1 subdomains

The subdomain structure of CTA1 is presented in Figure 1. The C-terminal $A1_3$ subdomain of CTA1 was originally thought to serve as the trigger for ERAD-mediated toxin translocation to the cytosol, but a $CTA1_{1–169}$ construct2 lacking most of the $A1_3$ subdomain could still move from the ER to the cytosol (21). This observation was consistent with a model of toxin translocation in which the ERAD system is activated by a global loss of structure in the isolated CTA1 subunit (11,20,21). We accordingly predicted that the $CTA1_{1–168}$ construct would, like the full-length construct, be thermally unstable. Biophysical measurements involving far-UV CD, fluorescence spectroscopy, and near-UV CD were conducted on CTA1 and $CTA1_{1–168}$ to test this prediction (Fig. 2 and Supporting Information Fig. S3). The loss of toxin structure with increasing temperature occurred for both full-length CTA1 (Figs. 2A–C) and $CTA1_{1–168}$ (Figs. 2D–F). Temperature-dependent changes to the toxin secondary structure were characterized with a T_m of 36°C for CTA1 and a T_m of 35°C $CTA1_{1–168}$; temperature dependencies of the peak fluorescence wavelength (λ_{max}) were characterized with a T_m of 35.5°C for CTA1 and a T_m of 35°C for $CTA1_{1–168}$; and temperature-induced changes to the toxin tertiary structure were characterized with a T_m of 32°C for CTA1 and a T_m of 32.5°C for $CTA1_{1–168}$ (Table 1). The similar transition temperatures of CTA1 and $CTA1_{1–168}$ suggested that truncation of the $CTA1_3$ subdomain had little effect on the thermal stability of CTA1.

It should be noted that the CD spectra of $CTA1_{1–168}$ exhibited a significantly weaker ππ* transition intensity between 200 and 210 nm and red-shifted nπ* bands compared to the full-

[2]In previous work (21), two variants of the $A1_3$ deletion construct were generated: His-tagged $CTA1_{1–168}$ was placed in a prokaryotic expression vector for protein purification, and $CTA1_{1–169}$ was placed in a eukaryotic expression vector for direct, plasmid-borne expression in the ER of transfected cultured cells.

length CTA1 molecule (Supporting Information Fig. S3). A relatively stronger ππ* signal is interpreted in terms of more twisted β-strands (23), and red-shifted nπ* bands indicate less polar environment (24). Our data therefore suggest that truncation of the $CTA1_3$ subdomain unwinds the twisted β-strands in the molecule, possibly accompanied with a tightening of its tertiary structure. The latter would cause a blue shift in tryptophan fluorescence spectra, which is indeed confirmed by the Trp fluorescence data which indicates a 3–4 nm blue-shifted spectra of $CTA1_{1–168}$ compared to those of CTA1 (Figs. 2B,E,J).

The near-UV CD spectra of CTA1 in the 250–300 nm region are generated by Tyr and Trp residues: CTA1 has no intramolecular disulfide bonds, and Phe side chains generate weaker bands at lower wavelengths (24,25). Full-length CTA1 demonstrates positive bands around 260 and 290 nm, most likely due to the L_b transitions of both Tyr and Trp residues, intervened with a broad negative band around 275 nm that can be assigned to the L_a transitions (Fig. 2C and Supporting Information Fig. S3C) (25). In the spectrum of $CTA1_{1–168}$, the negative (L_a) band becomes more pronounced (Fig. 2F and Supporting Information Fig. S3F), which may reflect conformational changes and the microenvironment of the aromatic amino acid side chains.

To determine the contribution of the $A1_2$ subdomain to CTA1 stability, additional biophysical measurements were performed on a $CTA1_{1–133}$ construct which lacked both the $A1_2$ and $A1_3$ subdomains (Figs. 2G–H and Supporting Information Figs. S3G–H). Near-UV CD measurements could not be accurately recorded for this construct. However, far-UV CD and fluorescence spectroscopy clearly demonstrated that $CTA1_{1–133}$ was less stable than either full-length CTA1 or $CTA1_{1–168}$ (Figs. 2I–J). $CTA1_{1–133}$ displayed a secondary structure T_m of 31°C, and the temperature dependence of its λ_{max} exhibited a T_m of 32°C (Table 1). These T_m values were, respectively, 5°C and 3.5°C lower than the corresponding T_m values for full-length CTA1. Thus, the $A1_2$ subdomain provides a degree of conformational stability to the catalytic $A1_1$ subdomain of CTA1. In addition, the CD spectra of $CTA1_{1–133}$ showed even weaker ππ* bands in comparison to $CTA1_{1–168}$ (Supporting Information Fig. S3). This may indicate a further relaxation of the β-strand twist in $CTA1_{1–133}$ and a larger spectral contribution from its α-helices.

CTA1 unfolding begins at the C-terminal subdomain

NMR measurements have shown that the C-terminus of CTA1 is partially unfolded even at 15°C (17). This suggests the overall loss of CTA1 structure that occurs with increasing temperature may begin with further unfolding of the $A1_3$ subdomain. To examine this possibility, we monitored the thermal unfolding of $CTA1_{1–168}$ in the presence of 10% glycerol (Fig. 3 and Supporting Information Fig. S4). Previous work has shown that glycerol blocks the thermal disordering of tertiary structure in the full-length CTA1 subunit (20). If the temperature-induced unfolding of CTA1 was initiated at its C-terminus, then glycerol would likely prevent the further loss of structure in the $CTA1_3$ subdomain. Truncation of the $CTA1_3$ subdomain would consequently eliminate the stabilizing effect of glycerol on the overall structure of CTA1. Consistent with this prediction, we found that $CTA1_{1–168}$ exhibited similar T_m values in either the absence or presence of 10% glycerol as determined by near-UV, far-UV CD, and fluorescence techniques (Table 1). The secondary and tertiary structural stability of $CTA1_{1–168}$ was therefore unaffected by glycerol treatment. In contrast, as determined by near-UV CD, exposure to glycerol resulted in a 5.5°C increase in the tertiary structure T_m for full-length CTA1 (20). It thus appears that the stabilizing effect of glycerol on CTA1 structure is mediated through an effect on the $A1_3$ subdomain. This observation further suggests that unfolding of the C-terminus precedes the global loss of CTA1 tertiary structure.

Acid-induced stabilization of CTA1

To further examine the processive unfolding of CTA1, we used a second experimental condition to stabilize the toxin structure. It has been reported that acidic pH prevents the thermal unfolding of ricin A chain (26). Furthermore, intoxication with either ricin or Shiga toxin is blocked at acidic pH because of an apparent inhibition of toxin export from the ER to the cytosol (27–30). Although the molecular basis of this effect was not determined, we hypothesized that acidic pH had a stabilizing effect on A chain structure which consequently disrupted toxin-ERAD interactions and A chain translocation to the cytosol. We therefore predicted that acidic pH would inhibit the thermal unfolding of CTA1.

CD and fluorescence spectroscopy were used to examine the effect of acidic pH on temperature-induced changes to the structure of CTA1 (Fig. 4 and Supporting Information Fig. S5). At pH 6.0, the thermal unfolding of CTA1 was characterized with a secondary structure T_m of 39°C, a λ_{max} T_m of 37°C, and a tertiary structure T_m of 38°C (Table 1). Thus, at acidic pH the T_m for CTA1 tertiary structure shifted to a higher temperature by 6°C. The thermal disordering of tertiary structure in a reduced CTA1/CTA2 heterodimer was also inhibited at pH 6.0 (Supporting Information Fig. S6, Table S2). Furthermore, cells bathed at acidic pH could deliver the CT holotoxin from the cell surface to the ER but could not export reduced CTA1 from the ER to the cytosol (Supporting Information Figs. S7–S8). These results, which were previously observed for glycerol-treated cells (20), strongly suggest that ERAD-mediated toxin translocation is triggered by a loss of CTA1 tertiary structure.

Acid-induced stabilization of CTA1 involves an effect on the C-terminal subdomain

Although acidic pH inhibited the thermal disordering of tertiary structure in full-length CTA1, it did not alter the thermal stability of $CTA1_{1–168}$ (Fig. 5 and Supporting Information Fig. S9). Both the tertiary and secondary structures of $CTA1_{1–168}$ exhibited nearly identical T_m values at pH 7.0 and pH 6.0, contrasting with the 6°C increase in tertiary structure T_m for full-length CTA1 at pH 6.0 as measured by near-UV CD (Table 1). The stabilizing effect of acidic pH on CTA1 tertiary structure thus appeared to involve the C-terminal $A1_3$ subdomain. This observation was consistent with the data derived from glycerol-treated toxin samples and again suggested that the thermal unfolding of CTA1 begins with a local loss of structure in the $A1_3$ subdomain.

DISCUSSION

In order to access the host cell cytosol, CTA1 undergoes what has been described as an order-disorder-order transition (17). The ordered CTA1 subunit travels from the cell surface to the ER as part of an intact CT holotoxin. In the ER, chaperone-assisted dissociation of reduced CTA1 from $CTA2/CTB_5$ releases the structural constraints on CTA1 unfolding and allows CTA1 to assume a disordered conformation which triggers its ERAD-mediated export to the cytosol (9,11,20). The translocated pool of CTA1 then interacts with cytosolic ADP-ribosylation factors and possibly other host factors to regain an active, ordered conformation (11,17). In this work, we examined the molecular details of CTA1 unfolding and identified the contribution of CTA1 subdomains to thermal disordering of the toxin.

A previous NMR study reported that a CTA1 construct lacking the C-terminal $A1_3$ subdomain retained the same core structure found in the full-length toxin (17). Likewise, $CTA1_{1–168/169}$ retained some enzymatic and biological activity (21). $CTA1_{1–168}$ also retained the same thermal stability as full-length CTA1 (Fig. 2,Table 1), which explains why the $CTA1_{1–169}$ construct was in a translocation-competent state (21). However, our data indicated that $CTA1_{1–133}$ was less stable than full-length CTA1: truncation of both the $A1_2$

and $A1_3$ subdomains reduced the secondary structure T_m by 5°C and the λ_{max} T_m by 3.5°C (Fig. 2, Table 1). This destabilization was not seen when only the $A1_3$ subdomain was removed from CTA1. Accordingly, we conclude that the $A1_2$ subdomain, which wraps around one face of the $A1_1$ subdomain, provides a degree of conformational stability to the catalytic core of the toxin.

As previously reported (11,20), the isolated CTA1 subunit was in a partially unfolded conformation at the physiological temperature of 37°C. The thermal disordering of CTA1 tertiary structure preceded the thermal perturbation of CTA1 secondary structure under control conditions. However, the thermal disordering of CTA1 tertiary structure was shifted to higher temperatures and occurred in tandem with the temperature-induced loss of CTA1 secondary structure when toxin samples were exposed to 10% glycerol (20) or pH 6.0 buffer (Fig. 4, Fig. S6, Table 1, Table S2). These effects were recorded with full-length CTA1 but not $CTA1_{1–168}$: neither glycerol nor acidic pH altered the thermal unfolding of $CTA1_{1–168}$ (Fig. 3, Fig. 5, Table 1). Collectively, these data indicated that the stabilizing effect of glycerol and acidic pH on CTA1 structure is mediated through an effect on the $A1_3$ subdomain. As an inhibition of unfolding in the $A1_3$ subdomain prevented the temperature-induced loss of structure in other regions of CTA1, it appears that the thermal unfolding of CTA1 begins with a localized loss of structure in the C-terminal domain. This event occurs after CTA1 dissociation from the holotoxin and may result, in part, from the loss of potentially stabilizing contacts between the $A1_3$ subdomain and CTA2.

The $A1_3$ subdomain itself was not required for toxin translocation to the cytosol (21). ERAD thus recognizes an unfolded region of CTA1 in the $A1_1$ and/or $A1_2$ subdomain(s). However, unfolding of the $CTA1_3$ subdomain preceded the loss of structure in other regions of CTA1. Forced stabilization of the $CTA1_3$ subdomain accordingly inhibited thermal unfolding of the $CTA1_1$ and $CTA1_2$ subdomains. This, in turn, blocked toxin-ERAD interactions and toxin translocation to the cytosol. These effects were first noted with glycerol (20) and were confirmed here with acidic pH, a second independent method of stabilizing CTA1 through an effect on the $A1_3$ subdomain.

We could not directly correlate the acid-induced inhibition of CTA1 translocation to an acid-induced inhibition of CT intoxication. Previous work has shown that experimentally induced alkalinization of the endosomes does not inhibit CT intoxication of cultured cells, but the effect of acidic conditions on CT intoxication was not examined (31). Here, initial control experiments found that cells incubated in acidified medium do not generate elevated levels of intracellular cAMP in response to treatment with forskolin, an agonist of adenlyate cyclase (data not shown). Since the ADP-ribosylation of Gsα by CTA1 leads to the activation of adenylate cyclase and high levels of intracellular cAMP, the acid-induced inhibition of adenylate cyclase activity prevented us from assessing the effect of acidic pH on CT intoxication. However, previous studies have shown that a block of toxin export from the ER to the cytosol will have a corresponding block on cellular intoxication (20,32,33).

Technical limitations also prevented us from monitoring the ER-to-cytosol translocation of $CTA1_{1–168}$ in cells exposed to 10% glycerol or acidic pH. Our data demonstrate that glycerol and acidic pH do not inhibit the thermal unfolding of $CTA1_{1–168}$, so glycerol and acidic pH would not be expected to block the ERAD-mediated translocation of $CTA1_{1–168}$. These potential experiments require a CT holotoxin containing the truncated $CTA1_{1–168}$ construct, but the cysteine residue linking CTA1 to CTA2/CTB_5 is missing from $CTA1_{1–168}$. Thus, it is not possible to incorporate $CTA1_{1–168}$ into a CT holotoxin.

Thermal instability in the catalytic CTA1 subunit appears to identify the toxin as a misfolded protein for ERAD-mediated translocation to the cytosol. To elucidate the

molecular details of this process, we have used glycerol and acidic pH as experimental conditions to alter the thermal unfolding of various CTA1 constructs. These conditions would not be found in the ER, but they were instead used to disrupt the normal biological process of CTA1 unfolding. With this approach we have provided mechanistic insight into the molecular mechanism of CTA1 unfolding, a key event for ERAD-mediated toxin translocation to the cytosol and cellular intoxication.

We previously suggested that the thermal stabilization of CTA1 may represent a novel therapeutic strategy (20). Here, we have more precisely identified the C-terminal $A1_3$ subdomain as a specific site where thermal unfolding of the CTA1 molecule is initiated. Specific stabilization of the $A1_3$ subdomain thus represents a possible therapeutic target. Inhibition of unfolding in the $A1_3$ subdomain prevents the temperature-induced loss of structure in other regions of CTA1. The stabilized conformation of CTA1 is not recognized as an ERAD substrate, which consequently prevents toxin translocation to the cytosol and productive intoxication. Thus, it should be possible to block the in vivo activity of CT with structure-based inhibitors of $A1_3$ unfolding.

Supplementary Material

Refer to Web version on PubMed Central for supplementary material.

REFERENCES

1. De Haan L, Hirst TR. Cholera toxin: a paradigm for multi-functional engagement of cellular mechanisms (Review). Mol. Membr. Biol. 2004; 21:77–92. [PubMed: 15204437]
2. Sanchez J, Holmgren J. Cholera toxin structure, gene regulation and pathophysiological and immunological aspects. Cell. Mol. Life Sci. 2008; 65:1347–1360. [PubMed: 18278577]
3. Zhang RG, Scott DL, Westbrook ML, Nance S, Spangler BD, Shipley GG, Westbrook EM. The three-dimensional crystal structure of cholera toxin. J. Mol. Biol. 1995; 251:563–573. [PubMed: 7658473]
4. O'Neal CJ, Jobling MG, Holmes RK, Hol WG. Structural basis for the activation of cholera toxin by human ARF6-GTP. Science. 2005; 309:1093–1096. [PubMed: 16099990]
5. O'Neal CJ, Amaya EI, Jobling MG, Holmes RK, Hol WG. Crystal structures of an intrinsically active cholera toxin mutant yield insight into the toxin activation mechanism. Biochemistry. 2004; 43:3772–3782. [PubMed: 15049684]
6. Lencer WI, Tsai B. The intracellular voyage of cholera toxin: going retro. Trends Biochem. Sci. 2003; 28:639–645. [PubMed: 14659695]
7. Majoul I, Ferrari D, Soling HD. Reduction of protein disulfide bonds in an oxidizing environment. The disulfide bridge of cholera toxin A-subunit is reduced in the endoplasmic reticulum. FEBS Lett. 1997; 401:104–108. [PubMed: 9013867]
8. Orlandi PA. Protein-disulfide isomerase-mediated reduction of the A subunit of cholera toxin in a human intestinal cell line. J. Biol. Chem. 1997; 272:4591–4599. [PubMed: 9020187]
9. Tsai B, Rodighiero C, Lencer WI, Rapoport TA. Protein disulfide isomerase acts as a redox-dependent chaperone to unfold cholera toxin. Cell. 2001; 104:937–948. [PubMed: 11290330]
10. Goins B, Freire E. Thermal stability and intersubunit interactions of cholera toxin in solution and in association with its cell-surface receptor ganglioside GM1. Biochemistry. 1988; 27:2046–2052. [PubMed: 3378043]
11. Pande AH, Scaglione P, Taylor M, Nemec KN, Tuthill S, Moe D, Holmes RK, Tatulian SA, Teter K. Conformational instability of the cholera toxin A1 polypeptide. J. Mol. Biol. 2007; 374:1114–1128. [PubMed: 17976649]
12. Surewicz WK, Leddy JJ, Mantsch HH. Structure, stability, and receptor interaction of cholera toxin as studied by Fourier-transform infrared spectroscopy. Biochemistry. 1990; 29:8106–8111. [PubMed: 2261465]

13. Teter K, Allyn RL, Jobling MG, Holmes RK. Transfer of the cholera toxin A1 polypeptide from the endoplasmic reticulum to the cytosol is a rapid process facilitated by the endoplasmic reticulum-associated degradation pathway. Infect. Immun. 2002; 70:6166–6171. [PubMed: 12379694]

14. Vembar SS, Brodsky JL. One step at a time: endoplasmic reticulum-associated degradation. Nat. Rev. Mol. Cell Biol. 2008; 9:944–957. [PubMed: 19002207]

15. Hazes B, Read RJ. Accumulating evidence suggests that several AB-toxins subvert the endoplasmic reticulum-associated protein degradation pathway to enter target cells. Biochemistry. 1997; 36:11051–11054. [PubMed: 9333321]

16. Rodighiero C, Tsai B, Rapoport TA, Lencer WI. Role of ubiquitination in retro-translocation of cholera toxin and escape of cytosolic degradation. EMBO Rep. 2002; 3:1222–1227. [PubMed: 12446567]

17. Ampapathi RS, Creath AL, Lou DI, Craft JW Jr, Blanke SR, Legge GB. Order-disorder-order transitions mediate the activation of cholera toxin. J. Mol. Biol. 2008; 377:748–760. [PubMed: 18272180]

18. Wernick NL, De Luca H, Kam WR, Lencer WI. N-terminal extension of the cholera toxin A1-chain causes rapid degradation after retrotranslocation from endoplasmic reticulum to cytosol. J. Biol. Chem. 2010; 285:6145–6152. [PubMed: 20056601]

19. Lord JM, Roberts LM, Lencer WI. Entry of protein toxins into mammalian cells by crossing the endoplasmic reticulum membrane: co-opting basic mechanisms of endoplasmic reticulum-associated degradation. Curr. Top. Microbiol. Immunol. 2005; 300:149–168. [PubMed: 16573240]

20. Massey S, Banerjee T, Pande AH, Taylor M, Tatulian SA, Teter K. Stabilization of the tertiary structure of the cholera toxin A1 subunit inhibits toxin dislocation and cellular intoxication. J. Mol. Biol. 2009; 393:1083–1096. [PubMed: 19748510]

21. Teter K, Jobling MG, Sentz D, Holmes RK. The cholera toxin A13 subdomain is essential for interaction with ADP-ribosylation factor 6 and full toxic activity but is not required for translocation from the endoplasmic reticulum to the cytosol. Infect. Immun. 2006; 74:2259–2267. [PubMed: 16552056]

22. Lavigne P, Crump MP, Gagne SM, Hodges RS, Kay CM, Sykes BD. Insights into the mechanism of heterodimerization from the 1H-NMR solution structure of the c-Myc-Max heterodimeric leucine zipper. J. Mol. Biol. 1998; 281:165–181. [PubMed: 9680483]

23. Woody, RW. Theory of circular dichroism of proteins. In: Fasman, GD., editor. Circular Dichroism and the Conformational Analysis of Biomolecules. New York and London: Plenum Press; 1996. p. 25-67.

24. Sreerama, N.; Woody, RW. Circular dichroism of peptides and proteins. In: Berova, N.; Nakanishi, K.; Woody, RW., editors. Circular Dichroism: Principles and Applications. Hoboken, NJ: John Wiley & Sons, Inc.; 2000. p. 601-620.

25. Woody, RW.; Dunker, AK. Aromatic and cysteine side-chain circular dichroism in proteins. In: Fasman, GD., editor. Circular Dichroism and the Conformational Analysis of Biomolecules. New York and London: Plenum Press; 1996. p. 109-157.

26. Argent RH, Parrott AM, Day PJ, Roberts LM, Stockley PG, Lord JM, Radford SE. Ribosome-mediated folding of partially unfolded ricin A-chain. J. Biol. Chem. 2000; 275:9263–9269. [PubMed: 10734065]

27. Sandvig K, Olsnes S. Entry of the toxic proteins abrin, modeccin, ricin, and diphtheria toxin into cells. II. Effect of pH, metabolic inhibitors, and ionophores and evidence for toxin penetration from endocytotic vesicles. J. Biol. Chem. 1982; 257:7504–7513. [PubMed: 7085634]

28. Sandvig K, Olsnes S, Brown JE, Petersen OW, van Deurs B. Endocytosis from coated pits of Shiga toxin: a glycolipid-binding protein from *Shigella dysenteriae* 1. J. Cell Biol. 1989; 108:1331–1343. [PubMed: 2564398]

29. Eiklid K, Olsnes S. Entry of *Shigella dysenteriae* toxin into HeLa cells. Infect. Immun. 1983; 42:771–777. [PubMed: 6358031]

30. Wesche J, Rapak A, Olsnes S. Dependence of ricin toxicity on translocation of the toxin A-chain from the endoplasmic reticulum to the cytosol. J. Biol. Chem. 1999; 274:34443–34449. [PubMed: 10567425]

31. Lencer WI, Strohmeier G, Moe S, Carlson SL, Constable CT, Madara JL. Signal transduction by cholera toxin: processing in vesicular compartments does not require acidification. Am. J. Physiol. 1995; 269:G548–G557. [PubMed: 7485507]

32. Teter K, Holmes RK. Inhibition of endoplasmic reticulum-associated degradation in CHO cells resistant to cholera toxin, *Pseudomonas aeruginosa* exotoxin A, and ricin. Infect. Immun. 2002; 70:6172–6179. [PubMed: 12379695]

33. Bernardi KM, Forster ML, Lencer WI, Tsai B. Derlin-1 facilitates the retro-translocation of cholera toxin. Mol. Biol. Cell. 2008; 19:877–884. [PubMed: 18094046]

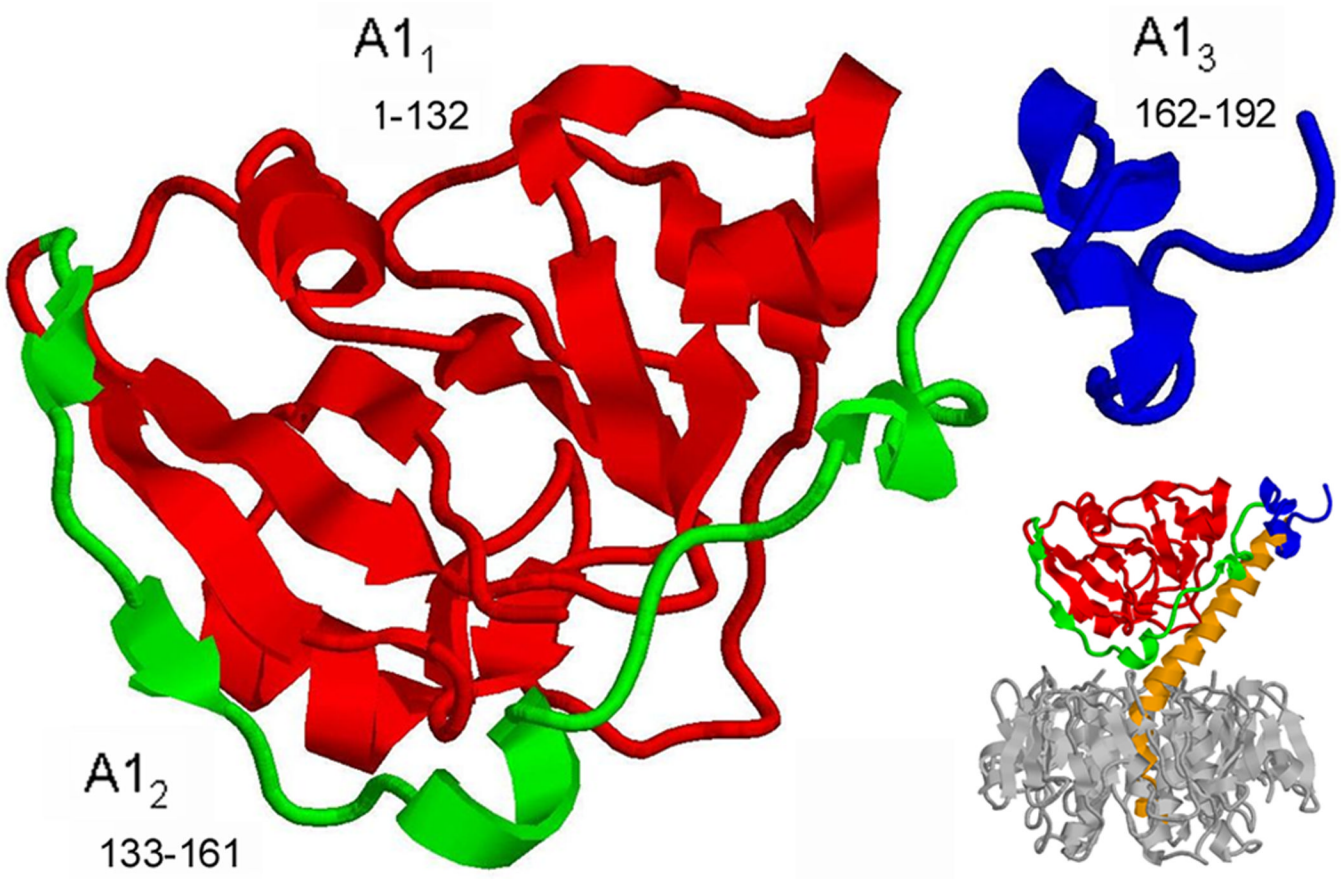

Figure 1.

Ribbon diagram of the CTA1 subunit. The presented structural model of the isolated CTA1 subunit is based upon the X-ray crystal structure of CT as determined by O'Neal *et al*. (Protein Data Bank entry 1S5F) (4). The subdomains, as described by Zhang *et al*. (3), are highlighted in different colors: the $A1_1$ subdomain is in red, the $A1_2$ subdomain is in green, and the $A1_3$ subdomain is in blue. Inset shows the orientation of CTA1 within the holotoxin, with CTA2 shown in orange and the B pentamer in grey. The images were generated using RasMol.

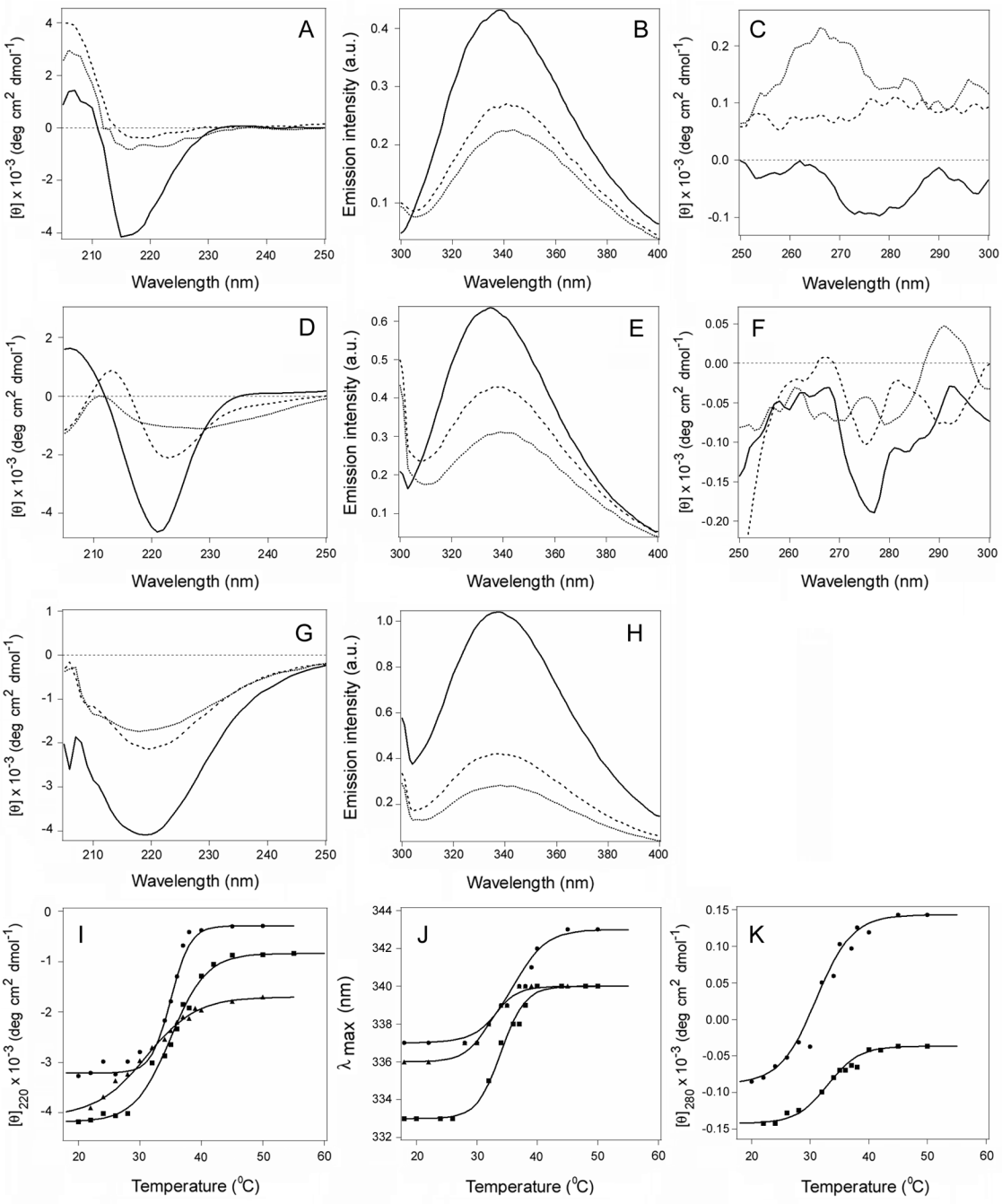

Figure 2.

Temperature-induced unfolding of CTA1, $CTA1_{1–168}$, and $CTA1_{1–133}$. (A–H): The thermal denaturation of CTA1 (A–C), $CTA1_{1–168}$ (D–F), or $CTA1_{1–133}$ (G–H) was monitored by far-UV CD (A, D, G), fluorescence spectroscopy (B, E, H), and near-UV CD (C, F). Spectra recorded at 18°C (solid line), 37°C (dashed line), and 50°C (dotted line) are shown. The full spectral profiles obtained over a temperature range from 18°C to 55°C are shown in Supporting Information Figure S3. (I–K): Thermal unfolding profiles for CTA1 (circles), $CTA1_{1–168}$ (squares), and $CTA1_{1–133}$ (triangles) were derived from data collected during the change in temperature from 18°C to 55°C. The experimental data points were fitted with theoretical curves simulated through Eq. 2–4, using the T_m and ΔH parameters summarized

in Tables 1 and S1. (I): For far-UV CD, the mean residue molar ellipticities at 220 nm ($[\theta]_{220}$) were plotted as a function of temperature. (J): For fluorescence spectroscopy, the maximum emission wavelengths were plotted as a function of temperature. (K): For near-UV CD analysis, the mean residue molar ellipticities at 280 nm ($[\theta]_{280}$) were plotted as a function of temperature.

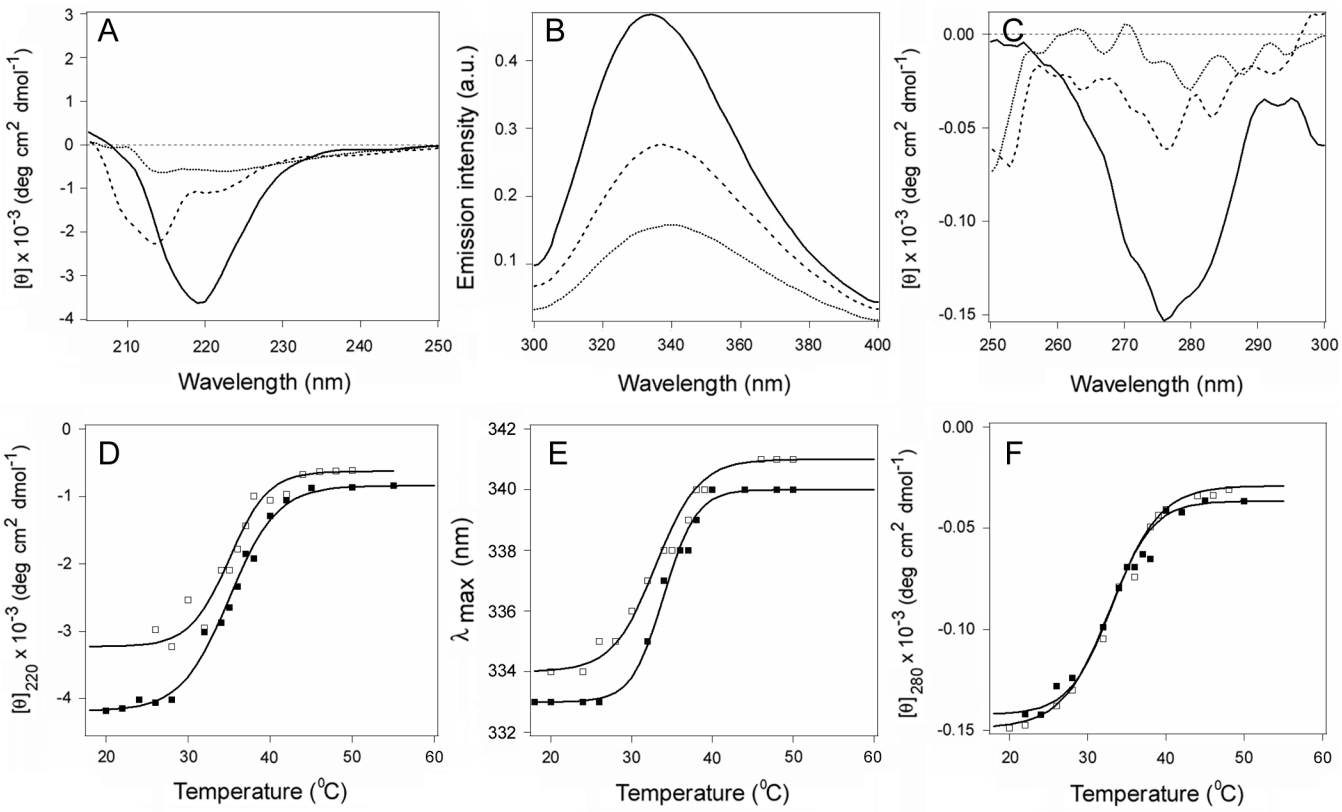

Figure 3.

Temperature-induced unfolding of $CTA1_{1–168}$ in the presence of 10% glycerol. (A–C): The thermal denaturation of $CTA1_{1–168}$ in the presence of 10% glycerol was monitored by far-UV CD (A), fluorescence spectroscopy (B), and near-UV CD (C). Spectra recorded at 18°C (solid line), 37°C (dashed line), and 50°C (dotted line) are shown. The full spectral profiles obtained over a temperature range from 18°C to 55°C are shown in Supporting Information Figure S4. (D–F): Thermal unfolding profiles for $CTA1_{1–168}$ in the absence (closed squares) or presence (open squares) of 10% glycerol were derived from the raw data presented in Supporting Information Figures S3D–F and S4, respectively. The experimental data points were fitted with theoretical curves simulated through Eq. 2–4, using the T_m and ΔH parameters summarized in Tables 1 and S1. (D): For far-UV CD, the mean residue molar ellipticities at 220 nm ($[\theta]_{220}$) were plotted as a function of temperature. (E): For fluorescence spectroscopy, the maximum emission wavelengths were plotted as a function of temperature. (F): For near-UV CD analysis, the mean residue molar ellipticities at 280 nm ($[\theta]_{280}$) were plotted as a function of temperature.

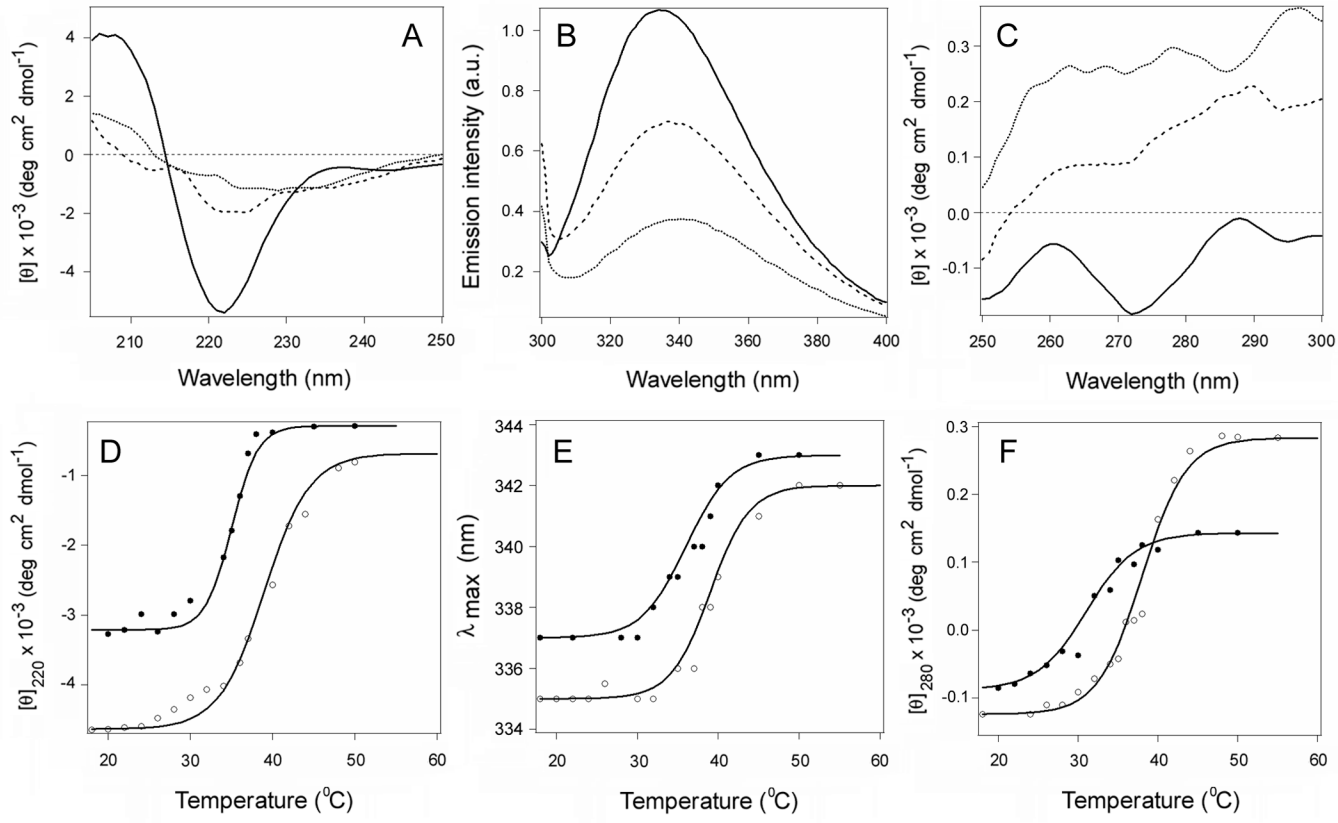

Figure 4.

Temperature-induced unfolding of CTA1 at acidic pH. (A–C): The thermal denaturation of CTA1 in pH 6.0 buffer was monitored by far-UV CD (A), fluorescence spectroscopy (B), and near-UV CD (C). Spectra recorded at 18°C (solid line), 37°C (dashed line), and 50°C (dotted line) are shown. The full spectral profiles obtained over a temperature range from 18°C to 55°C are shown in Supporting Information Figure S5. (D–F): Thermal unfolding profiles for CTA1 in pH 7.0 buffer (closed circles) or pH 6.0 buffer (open circles) were derived from the raw data presented in Supporting Information Figures S3A–C and S5, respectively. The experimental data points were fitted with theoretical curves simulated through Eq. 2–4, using the T_m and ΔH parameters summarized in Tables 1 and S1. (D): For far-UV CD, the mean residue molar ellipticities at 220 nm ($[\theta]_{220}$) were plotted as a function of temperature. (E): For fluorescence spectroscopy, the maximum emission wavelengths were plotted as a function of temperature. (F): For near-UV CD analysis, the mean residue molar ellipticities at 280 nm ($[\theta]_{280}$) were plotted as a function of temperature.

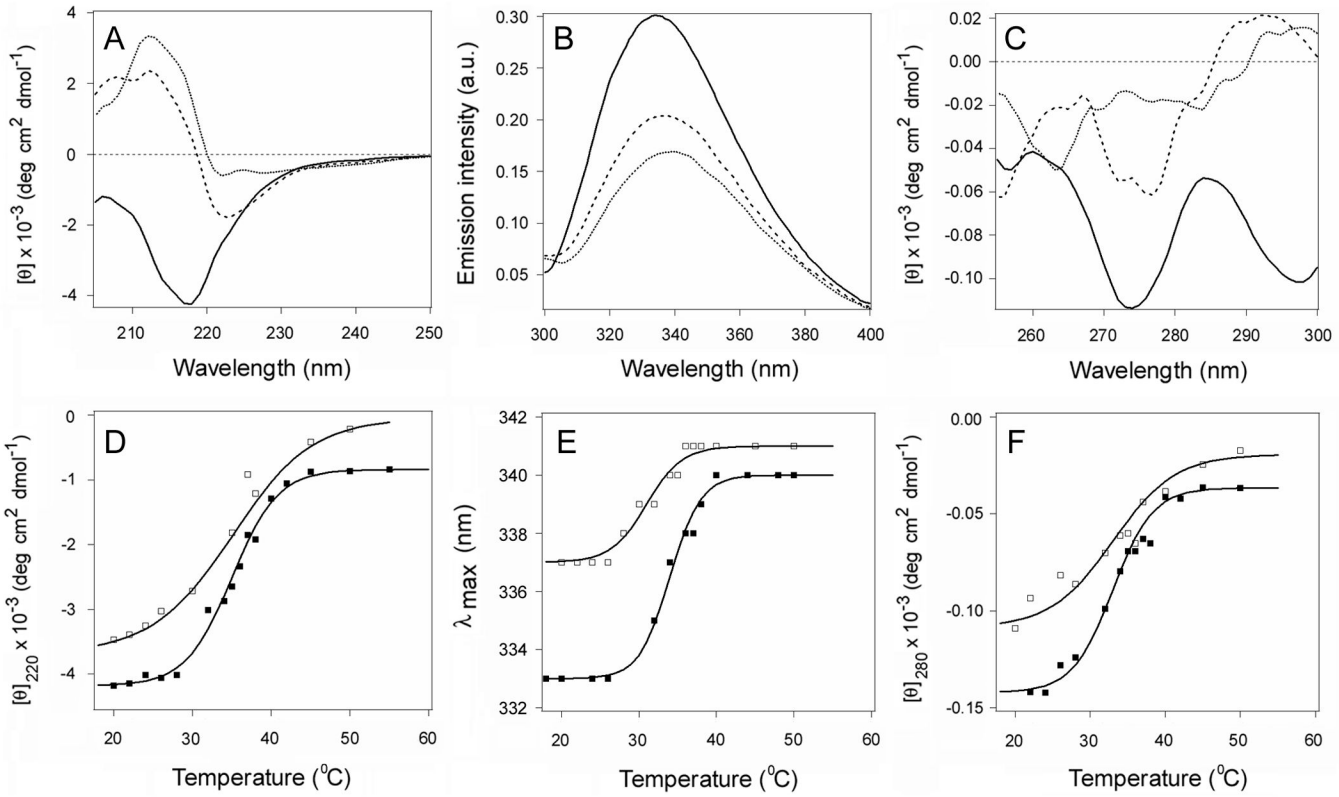

Figure 5.

Temperature-induced unfolding of $CTA1_{1–168}$ at acidic pH. (A–C): The thermal denaturation of $CTA1_{1–168}$ pH 6.0 buffer was monitored by far-UV CD (A), fluorescence spectroscopy (B), and near-UV CD (C). Spectra recorded at 18°C (solid line), 37°C (dashed line), and 50°C (dotted line) are shown. The full spectral profiles obtained over a temperature range from 18°C to 55°C are shown in Supporting Information Figure S9. (D–F): Thermal unfolding profiles for $CTA1_{1–168}$ in pH 7.0 buffer (closed squares) or pH 6.0 buffer (open squares) were derived from the raw data presented in Supporting Information Figures S3D–F and S9, respectively. The experimental data points were fitted with theoretical curves simulated through Eq. 2–4, using the T_m and ΔH parameters summarized in Tables 1 and S1. (D): For far-UV CD, the mean residue molar ellipticities at 220 nm ($[\theta]_{220}$) were plotted as a function of temperature. (E): For fluorescence spectroscopy, the maximum emission wavelengths were plotted as a function of temperature. (F): For near-UV CD analysis, the mean residue molar ellipticities at 280 nm ($[\theta]_{280}$) were plotted as a function of temperature.

Table 1

Thermal stabilities of CTA1 and the CTA1 deletion constructs.[a]

	T_m (°C)		
	far-UV CD	**λ_{max}**	**near-UV CD**
CTA1	36	35.5	32
CTA1 pH 6.0	39	37	38
$CTA1_{1–168}$	35	35	32.5
$CTA1_{1–168}$ + glycerol	35	33	33
$CTA1_{1–168}$ pH 6.0	35	34	32
$CTA1_{1–133}$	31	32	--

[a] T_m values were calculated from the thermal unfolding profiles presented in Figures 2–5. Unless otherwise noted, experiments were performed at pH 7.0